

# In Vivo Magnetic Resonance Imaging of Single Cells in Mouse Brain with Optical Validation

Chris Heyn,<sup>1,2\*</sup> John A. Ronald,<sup>1,3</sup> Lisa T. Mackenzie,<sup>3,4</sup> Ian C. MacDonald,<sup>3</sup>  
Ann F. Chambers,<sup>3,4</sup> Brian K. Rutt,<sup>1,3</sup> and Paula J. Foster<sup>1,3</sup>

**In the current work we demonstrate, for the first time, that single cells can be detected in mouse brain in vivo using magnetic resonance imaging (MRI). Cells were labeled with superparamagnetic iron oxide nanoparticles and injected into the circulation of mice. Individual cells trapped within the microcirculation of the brain could be visualized with high-resolution MRI using optimized MR hardware and the fast imaging employing steady state acquisition (FIESTA) pulse sequence on a 1.5 T clinical MRI scanner. Single cells appear as discrete signal voids on MR images. Direct optical validation was provided by coregistering signal voids on MRI with single cells visualized using high-resolution confocal microscopy. This work demonstrates the sensitivity of MRI for detecting single cells in small animals for a wide range of application from stem cell to cancer cell tracking. Magn Reson Med 55:23–29, 2006. © 2005 Wiley-Liss, Inc.**

**Key words:** Magnetic resonance imaging; iron oxide; single cell; FIESTA

The capacity to track specific cells and cell populations noninvasively over time in animals and humans will have a tremendous impact on our ability to study, diagnose, and treat disease. Currently, a number of imaging modalities have been developed for tracking cells in vivo, including positron emission tomography, single photon computed tomography, optical techniques, and magnetic resonance imaging (MRI) (1). Of these, MRI may have the most exciting potential for resolving soft tissue structures in three dimensions, deep within optically opaque tissues, at very high spatial resolution (of order 100  $\mu\text{m}$  voxel size in each of three dimensions), while simultaneously being able to detect trace quantities of magnetic label and without the use of ionizing radiation. MRI of superparamagnetic iron oxide (SPIO)-labeled cells, in particular, has found numerous applications over the past few years in both basic science research and clinical medicine. These include

tracking of stem cells, tumor cells, T-lymphocytes, dendritic cells, and macrophages in a variety of conditions such as stroke, multiple sclerosis, spinal cord injury, atherosclerosis, and organ transplantation and rejection (2). Nevertheless, one of the major criticisms leveled at MRI has been that it is intrinsically a low-sensitivity imaging modality in the context of detecting labeled cells or molecules. This perception has arisen mainly because most previous MR cell tracking studies have used relatively large numbers of cells ( $10^5$ – $10^6$  cells), as well as the generally held opinion that MRI is sensitive to molecular concentrations in the tens of micromolar to millimolar range (3). While the ability of MRI to visualize thousands or millions of SPIO-labeled cells has attracted much attention in the past few years, the imaging of large groups of cells does not provide a precise knowledge of individual cell phenotype. In addition, certain biologic processes such as stem cell migration and homing and cancer cell invasion and metastasis require the ability to track smaller numbers of cells or even single cells. In vivo detection of single cells by MRI would represent a major advance in the field of cellular and molecular imaging and would enable many new fundamental biologic investigations.

Toward this goal, there has been recent effort to assess and decrease the detection limit of cellular MRI, primarily by using dedicated small-animal MRI scanners operating at very high magnetic field and employing imaging pulse sequences that produce contrast dependent on either  $T_2$  or  $T_2^*$  relaxation times. Using a model of direct cerebral injection of SPIO-labeled embryonic stem (ES) cells into rat brain, Hoehn et al. demonstrated an in vivo detection limit of 500 cells at 7 T (4). More recently, Stroh et al. established an in vivo detection limit of 100 SPIO-labeled ES cells in rat brain at 17.6 T (5). MRI detection of single cells has been demonstrated in vitro. In 1999, Dodd et al. were the first to show that single SPIO-labeled T-lymphocytes could be detected in gelatin at 7 T (6). Single cell detection has since been demonstrated by other groups in vitro (7–9) as well as in a fixed excised embryo at 7 T (10). Although those studies have required high magnetic fields, our group has demonstrated that in vitro single cell detection is possible at a clinical MRI field strength of 1.5 T (11).

Recently, there have been two separate reports of in vivo single cell detection in mouse liver (12) and mouse heart (13). Due to the difficulty in correlating single cells detected in MR images with histology in these organs, the authors used indirect lines of evidence to prove single cell detection. This evidence included a comparison of the MR contrast generated for single cells in vitro and in vivo and histologic analyses, which showed that solitary SPIO-labeled cells are present throughout the liver and sufficiently separated in space to ensure that single cells were

<sup>1</sup>Imaging Research Laboratories, Robarts Research Institute, London, Ontario, Canada.

<sup>2</sup>Institute of Medical Science, University of Toronto, Toronto, Ontario, Canada.

<sup>3</sup>Department of Medical Biophysics, University of Western Ontario, London, Ontario, Canada.

<sup>4</sup>London Regional Cancer Program, London, Ontario, Canada.

Grant sponsor: Canadian Institutes for Health Research; Grant numbers: 42511 (AFC and ICM) and 57916 (PJF and BKR); Grant sponsor: Barnett-Lvey Heart and Stroke Foundation of Ontario; Grant sponsor: MS Society of Canada Donald Paty Career Award; Grant sponsor: CIHR.

\*Correspondence to: Chris Heyn, Imaging Research Laboratories, Robarts Research Institute, 100 Perth Drive, London, Ontario N6A 5K8, Canada. E-mail: cheyn@imaging.robarts.ca

Received 27 June 2005; revised 14 August 2005; accepted 14 September 2005.

DOI 10.1002/mrm.20747

Published online 8 December 2005 in Wiley InterScience (www.interscience.wiley.com).

present in any given voxel. In the current work, we show for the first time that single cells can be detected in mouse brain *in vivo* and provide direct optical validation of single cell detection. We have demonstrated this for a macrophage cell line that was labeled with SPIO *in vitro*, disseminated into mouse brain via intracardiac injection, and imaged using optimized gradient hardware and a balanced SSFP pulse sequence FIESTA (also known as balanced fast field echo or trueFISP) at 1.5 T. Animals that received SPIO-labeled macrophages exhibited a small number of discrete areas of low signal intensity (heretofore termed “signal voids”) on MR images. To determine the source of these signal voids, that is whether they arise from single cells or multiple cells, coregistration of *in vivo* MRI, *ex vivo* MRI, and high-resolution confocal microscopy was performed. This work corroborates the *in vivo* single cell detection limit described by others and demonstrates the potential of MRI for cell tracking at the single cell level with obvious applications to the study of stem cell, cancer cell, and immune cell trafficking.

## METHODS

### Cell Labeling

J774 cells (ATCC, Manassas, VA, USA), a macrophage cell line derived from BALB/c mice, were maintained in Dulbecco’s modified Eagle’s medium (DMEM) containing 10% fetal bovine serum (FBS) at 37°C and 5% CO<sub>2</sub>. For SPIO labeling, 2 × 10<sup>6</sup> cells were plated and supplemented with DMEM containing 10% FBS and 112 μg Fe/mL Feridex IV (Berlex Laboratories, Wayne, NJ, USA) for 24 h. Cells were washed thoroughly with phosphate-buffered saline (PBS) to remove unincorporated SPIO and counted using a hemacytometer. Cell viability was assessed using Trypan blue exclusion. Cell suspensions were labeled with the lipophilic carbocyanine fluorescent dye, DiI (1,1-dioctadecyl-3,3,3’,3’-tetramethylindocarbocyanine perchlorate) (Molecular Probes, Eugene, OR, USA) by incubating SPIO-labeled cells with 5 μM DiI in serum-free DMEM for 20 min at 37°C. A portion of the labeled cells (1 × 10<sup>6</sup>) was suspended in gelatin in 5-mm glass NMR tubes for measurements of cellular iron uptake. The mean cellular SPIO content, expressed in picograms of Fe per cell, was assessed using a susceptometry technique, the Reilly McConnell–Meisenheimer method modified for multiecho imaging (14).

### Animal Preparation

To deliver SPIO-labeled cells into the mouse brain, cells were injected into the left ventricle of the beating mouse heart—a technique commonly used to deliver cells via the arterial circulation to various organs in the mouse. Female C57BL/6 mice (5 weeks old, *n* = 6) (Charles River Laboratories, Wilmington, MA, USA) were cared for in accordance with standards of the Canadian Council on Animal Care and under an approved protocol of the University of Western Ontario’s Council on Animal Care. Mice were first anesthetized with an intraperitoneal (i.p.) injection of ketamine/xylazine (100/20 mg/mL) at a dose of 0.03 mL/10 g. A small incision was made midline through the superficial skin exposing the second, third, and fourth ribs. A 27-

gauge needle on the end of a sterile catheter was inserted between the third and fourth ribs perpendicular to the sternum. A 0.1-mL suspension of SPIO-labeled J774 cells (10,000 cells) was then injected into the left ventricle over 10 s. The small incision to the superficial skin was sutured closed.

### Magnetic Resonance Imaging

All MRI was performed on a 1.5 T GE CV/i whole-body clinical MR scanner using a custom-built gradient coil (inner diameter 12 cm, maximum gradient strength 600 mT/m, and peak slew rate 2000 T/m/s). Within 5 h after the cell injection, mice were anesthetized with isoflurane (1% in 100% oxygen) and positioned in a custom-built solenoidal mouse head radiofrequency coil (1.5 cm diameter). The small diameter of the RF coil immobilized the mouse head and restricted movement. The coil was housed within a Plexiglas chamber equipped with ports for inhalational anesthesia and a warm water heating system to maintain body temperature during the imaging session. The RF coil was then positioned within the gradient coil insert in the scanner. *In vivo* images were obtained using the 3D FIESTA pulse sequence (FOV = 2 × 2 cm, TR/TE 7.0/3.4 ms, flip angle 30°). The scanned resolution was 100 × 100 × 200 μm<sup>3</sup>. Zero filling was used to give an interpolated voxel dimension of 39 × 39 × 100 μm<sup>3</sup>. All resolutions stated in this paper refer to the scanned resolution. The total acquisition time was 1.5 h and the SNR was 60.

Immediately following *in vivo* MRI, mice were sacrificed by an i.p. injection of pentobarbital (Euthanyl) followed by an incision into the right atrium to drain blood. Animals were not perfused in order to prevent washing through of SPIO-labeled cells. Mouse brains were excised and placed in formalin for 48 h. For imaging, mouse brains were placed in 1-cm-diameter plastic tubes immersed in Fluorinert (3M, Minneapolis, MN, USA), a perfluorocarbon ether that does not have any MR signal. *Ex vivo* mouse brain FIESTA images were acquired at 100 × 100 × 200 and/or 100 × 100 × 100 μm<sup>3</sup> resolution (interpolated voxel dimensions of 39 × 39 × 100 and 39 × 39 × 50 μm<sup>3</sup>, respectively). Signal averaging (NEX) was adjusted so that the SNR of the *ex vivo* images was matched to that of the *in vivo* images (60). The 100 × 100 × 200 μm<sup>3</sup> *ex vivo* images were obtained with 9 NEX in 26 min and the 100 × 100 × 100 μm<sup>3</sup> *ex vivo* images were obtained with 36 NEX in 2 h.

The amount of MR contrast for a given signal void generated by a SPIO-labeled cell *in vivo*, and *ex vivo* was assessed by calculating the fractional signal loss ( $\Delta S/S$ ). This was calculated by taking the difference between the signal from the central voxel of the void ( $S_{\text{cell}}$ ) and signal from background brain containing no cells ( $S$ ) ( $\Delta S = S - S_{\text{cell}}$ ) and dividing by the background signal. The contrast-to-noise ratio (CNR) was calculated from  $\Delta S/S$ :  $\text{CNR} = (\Delta S/S) \cdot \text{SNR}$ .

### Confocal Microscopy and Coregistration with MRI

To determine the number of cells contributing to signal voids visualized with MRI, confocal microscopy and

coregistration with MRI were performed on mouse brains. Mouse brains were cryopreserved in ascending concentrations of sucrose (10, 20, and 30%) in distilled water for 1 h each. Brains were immersed in OCT compound, oriented in a sectioning plane parallel to that of MR imaging, and frozen using liquid nitrogen. Contiguous 25- $\mu\text{m}$  frozen sections were collected through the entire mouse brain. Frozen sections were used to minimize distortion effects and fixation artifacts associated with paraffin embedding. Sections were assessed for the presence of DiI-labeled cells using epifluorescent microscopy. Sections containing DiI (wavelength 549 nm)-labeled cells were then imaged at low magnification using a Zeiss 510 laser scanning confocal microscope. Differential interference contrast (DIC) images were taken to give reference to the location in the brain where each cell was located. Due to a disparity in slice thickness, a methodology for spatially aligning the MR and optical data that allowed for direct correlation of single cells was developed. This registration was facilitated by the abundance of anatomic landmarks in the brain that are visible in both MRI and optical imaging. One such landmark is the anterior commissure (ac), a white matter tract that connects the left and right hemispheres caudally and diverges into two distinct bundles rostrally (Fig. 2a). The divergence of the ac, which occurs over one MR slice and over three 25- $\mu\text{m}$  histologic sections, was used to register the MR and confocal data. For this reason, signal voids were selected for correlation with confocal microscopy from the neighborhood of this ac divergence. Each area of DiI fluorescence was correlated with signal voids in MR images. High magnification optical z-sectioning (0.7  $\mu\text{m}$  optical section) throughout regions containing DiI-labeled cells was also performed to confirm the presence of single cells or determine the number of cells in any given area of DiI fluorescence. 3D surface rendering of the z-section confocal data was performed using OsiriX to visualize the morphology of single cells.

## RESULTS

1774 macrophages were chosen for single cell detection experiments because they can be reproducibly labeled with SPIO nanoparticles at very high loading levels. For the SPIO concentration and labeling time used, the average cellular SPIO content was  $60.9 \pm 1.6$  pgFe/cell, which is 2 to 3 times greater than the highest loading achieved with Feridex in most other cell lines (15).

While most studies that have investigated the detection limits of SPIO-labeled cells have examined cells that were locally implanted into tissue (4,5), the left ventricular (LV) delivery of cells, as used here, is a good model for studying in vivo single cell detection because the cells distributed systemically by the arterial circulation are delivered to the brain and other organs as single cells, where they become arrested in the capillaries of the microcirculation. Cell delivery into a given organ is initially proportional to the percentage of cardiac output (CO) to the organ. For mouse brain, the %CO to the brain is  $\sim 10\%$  (16). For 10,000 cells, 1000 cells are expected to be delivered to the brain microcirculation. Studies on injected tumor cells, however, indicate that cells are not efficiently retained in the first organ bed they encounter but gradually accumulate in the

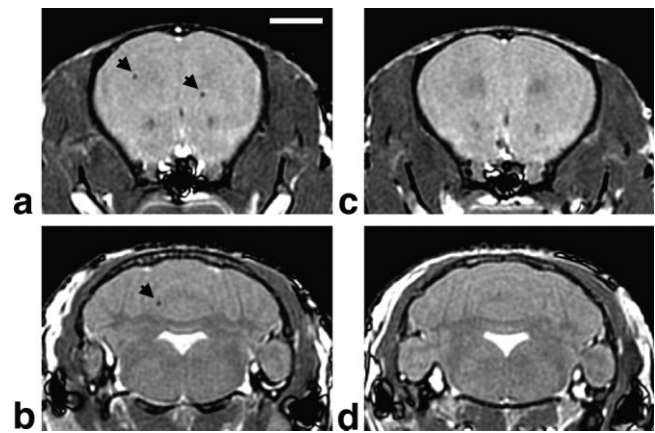


FIG. 1. In vivo MRI comparing mouse brains from an animal that received left ventricle intracardiac injection of SPIO-labeled macrophages and a control animal that did not. FIESTA MR images from animals injected with SPIO-labeled cells show a number of areas of low signal intensity (signal voids) throughout the brain consistent with SPIO-induced signal loss. (a) Two signal voids (black arrows) in the frontal cortex. (b) One signal void in the cerebellum. Corresponding MR images from the frontal cortex (c) and cerebellum (d) of the control show no evidence of SPIO-induced signal voids. Scale bar (a) 2 mm.

liver and lungs. By 2 h postinjection,  $<0.2\%$  of the injected cell fraction is expected to be retained in the brain (16).

On average,  $28 \pm 3$  discrete, punctate signal voids were visualized throughout the brains in MR images from the six animals injected with 10,000 SPIO-labeled macrophages (Figs. 1a and b). The number of signal voids is consistent with the expected number of cells in the mouse brain (0.2–0.3% of the total number of cells injected). No signal voids were visible in brains from control mice that received no cells (Figs. 1c and d). For in vivo imaging, signal voids measured on average six interpolated voxels (294  $\mu\text{m}$ ) in diameter and spanned an average of three interpolated MR slices (300  $\mu\text{m}$ ). The area of MR signal loss is substantially larger than the dimension of the cell ( $\sim 15$   $\mu\text{m}$  diameter) and is consistent with the “blooming effect” typically observed for single SPIO-labeled cells in vitro (6,9,11).

Three regions of signal void, in the vicinity of the divergence of the ac, are shown in another representative in vivo mouse brain image (Fig. 2a). One signal void is located in the caudate putamen (CPu) and two are located superior to the corpus callosum (cc). Figures 2b–d show ex vivo images of the same brain at the same resolution as the in vivo scan ( $100 \times 100 \times 200$   $\mu\text{m}^3$ , Fig. 2b) and at higher resolution ( $100 \times 100 \times 100$   $\mu\text{m}^3$ , Figs. 2c and d). The number of signal averages in the image acquisition was varied so that the SNR of all images was equal. The three regions of signal void are detected in the same locations in the in vivo and ex vivo images acquired at  $100 \times 100 \times 200$   $\mu\text{m}^3$  resolution (Figs. 2a and b), indicating that the cells were not washed through during the exsanguination process. In the highest resolution ex vivo image, the three signal voids appear in the same in-plane locations but span a total of 10 MR slices (500  $\mu\text{m}$ ). Two MR slices

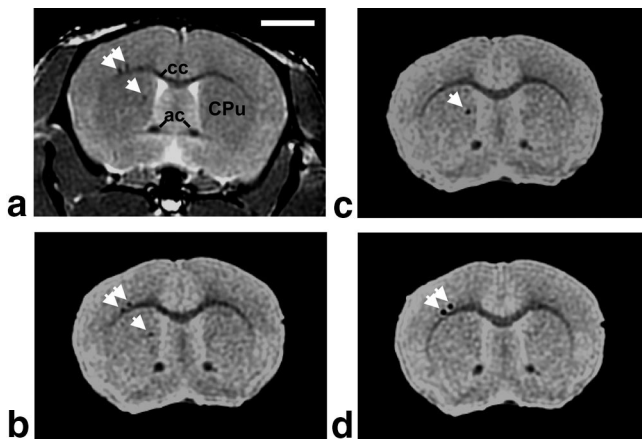


FIG. 2. In vivo and ex vivo MRI of a mouse brain from an animal injected with SPIO-labeled macrophages. (a) In vivo MRI showing three signal voids ( $100 \times 100 \mu\text{m}^2$  in plane,  $200\text{-}\mu\text{m}$  slice thickness). (b) Ex vivo MRI at the same resolution and slice location as (a) showing the same three signal voids. (c, d) High-resolution ex vivo MRI ( $100 \times 100 \mu\text{m}^2$  in plane,  $100\text{-}\mu\text{m}$  slice thickness). The three signal voids in (a) and (b) now appear in two different MR slices. cc, corpus callosum. ac, anterior commissure. CPu, caudate putamen. Scale bar (a) 2 mm.

containing these signal voids are shown (Figs. 2c and d). The signal minima for the two signal voids above the cc appear on a MR slice located 5 slices ( $\sim 250 \mu\text{m}$ ) rostral to the MR slice containing the signal minima for the void in the CPu.

The signal voids are clearly easier to detect in the highest resolution images (Figs. 2c and d). The average  $\Delta S/S$  values for all signal voids ( $n = 20$ ) detected in vivo and ex vivo reflect this improved detection, with  $\Delta S/S$  values approximately doubling in the highest resolution ex vivo images ( $0.483 \pm 0.023$ ) compared to the lower resolution in vivo ( $0.227 \pm 0.014$ ) and ex vivo images ( $0.280 \pm 0.015$ ). There is also a significant difference in the  $\Delta S/S$  values for signal voids measured in vivo and ex vivo at the same resolution (paired samples  $t$  test,  $df = 19$ ,  $P < 0.01$ ).

To determine the source of signal voids on MRI (e.g., single cell, multiple cells, or artifact), histologic comparison was performed on contiguous  $25\text{-}\mu\text{m}$  sections taken from the rostral portion of the mouse brain corresponding to the divergence of the ac. Low- and high-magnification z-section confocal microscopy of sections containing labeled cells was performed to locate cells in the brain and assess how many cells were present at each location, respectively. Importantly, every cell detected by confocal microscopy was represented by a corresponding signal void on both in vivo and ex vivo MRI. In Fig. 3 the three signal voids in the high-resolution ex vivo MRI (Figs. 2c and d) are compared with the corresponding DiI fluorescence on low-magnification confocal microscopy. The DiI fluorescence corresponding to the cell in the CPu was localized in one  $25\text{-}\mu\text{m}$  optical section (Figs. 3b and c). Twelve histologic sections ( $\sim 300 \mu\text{m}$ ) rostral to this, two areas of DiI fluorescence above the cc were detected on two contiguous  $25\text{-}\mu\text{m}$  sections (Figs. 3e and f; only one section is shown). There is good agreement between the spatial location (both in-plane and MR slice) of signal voids on

MR images and regions of DiI fluorescence visualized using confocal microscopy.

Finally, high-magnification optical z-sectioning ( $0.7 \mu\text{m}$  optical section) of regions containing DiI fluorescence was performed using confocal microscopy to resolve individual cells. For the region of DiI fluorescence in the CPu, optical z-sectioning shows a single cell with DiI accumulation (red) in the cytoplasm and cell membrane and the presence of a solitary nucleus (n) devoid of DiI (Fig. 4a). Optical z-sectioning is also shown for one of the two cells above the cc, spanning the two contiguous sections within which the cells appeared (z-sectioning for the two contiguous sections is shown on two separate rows) (Fig. 4b). In this example, a single nucleus that appears on one histologic section (top row) and continues on the contiguous section (bottom row) suggests the presence of a single cell. 3D surface rendering of the z-section data indicates that this single cell is trapped at the bifurcation of a  $6\text{-}\mu\text{m}$  capillary (last column in Fig. 4b).

## DISCUSSION

The results of single cell detection with J774 macrophages described herein should be transferable to other cell types, as the physics of single cell MRI is indifferent to cell type or labeling technique as long as the intracellular iron label is in the superparamagnetic form (14). We have demonstrated in vivo single cell detection at a SPIO loading of  $60.9 \pm 1.6 \text{ pg Fe/cell}$ , a relatively high loading level for Feridex nanoparticles that can easily be achieved in phagocytic cells such as macrophages but would be more difficult in nonphagocytic cells. Over the past few years, the efficiency of labeling nonphagocytic cells with SPIO nanoparticles has improved significantly. For instance, DNA transfection agents complexed with SPIO nanoparticles (15), or SPIO conjugated to HIV-tat protein (7), have been used to label lymphocytes, stem cells, and tumor cells with SPIO in the  $10\text{--}30 \text{ pg Fe/cell}$  range. More recently, micrometer-size iron oxide particles (MPIO) have been used to label nonphagocytic cells at iron loading levels that are similar to that used in our experiments ( $\sim 100 \text{ pg Fe/cell}$ ) (9). Further improvements in nanoparticle labeling or the use of MPIOs should provide sufficient SPIO labeling to allow the detection of nonphagocytic cells at the single cell level.

The proof of single cell detection by MRI requires some form of validation because of the lack of specificity of negative contrast MR techniques. For example, other sources of magnetic field inhomogeneity (e.g., blood) can cause localized MR signal loss and mimic the appearance of SPIO-labeled cells with  $T_2\text{-}$  and  $T_2^*\text{-}$ weighted pulse sequences. The presence of signal voids in animals receiving SPIO-labeled cells compared to control animals suggests that this is not likely the case in the brain regions examined in our experiments (Fig. 1). However, the intrinsically low imaging resolution of MRI compared to the dimension of a SPIO-labeled cell does not preclude the possibility that multiple cells can reside within a given imaging voxel and mimic the appearance of a single cell. Coregistration of histology with MR images is therefore essential to unambiguously assign a given single void to a single cell.

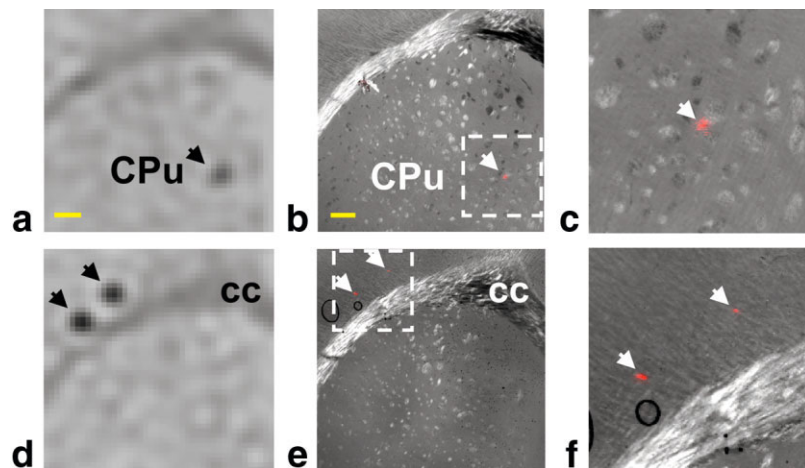


FIG. 3. Correlation of cells detected by ex vivo MRI and low-magnification confocal microscopy. (a) Magnified view of MRI (Fig. 2c) showing a signal void (black arrow) in the caudate putamen (CPu). (b) Corresponding low-magnification confocal image (overlay of differential interference contrast (DIC) and Dil fluorescence image) from a histologic section corresponding to MRI in (a). There is good correlation between the signal void in (a) and the area of Dil fluorescence in (b) (white arrow), as well as anatomic landmarks between the MR and optical image. (c) Magnification of the area of Dil fluorescence indicated by the white box in (b). (d) Magnified view of MRI (Fig. 2d) showing two signal voids (black arrows) superior to the corpus callosum (cc). (e) Corresponding confocal image corresponding to the MRI shown in (d). There is good correlation between the two signal voids in MRI and the two areas of Dil fluorescence (white arrows). (f) Magnified view of Dil fluorescence from the region of interest defined by the white box in (e). Scale bar (a,b) 200  $\mu\text{m}$ .

Coregistration of histology and MRI is not a simple task. Beside the disparity in slice thickness, other problems such as tissue distortion that occurs when live tissue is fixed and sectioned can also complicate the process. The single cell detection and confirmation task was simplified first by selecting an organ that was well suited for coregistration of MRI and histologic data. The brain contains many anatomic landmarks that can be used to guide the registration. To minimize the discrepancy in slice thickness and tissue distortion that occurs between in vivo MRI

and histology, we performed ex vivo MRI as an intermediate step that allowed us to generate higher resolution MR images, completely free of any motion effects. Finally, the small number of cells that were used and LV-injection method of delivery to the brain ensured a greater probability of finding a unique pattern of single cells that could be unambiguously detected using MRI and correlated with histology.

While we have not undertaken a rigorous analysis of the sensitivity and specificity of single cell detection in this

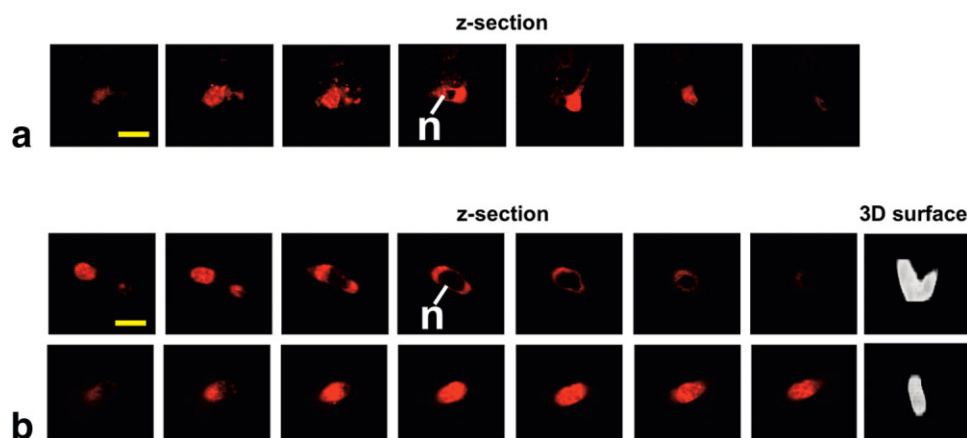


FIG. 4. High-magnification confocal microscopy validation of single cell detection. Confocal z-sectioning (0.7- $\mu\text{m}$  optical section) was performed on regions of Dil fluorescence located by low-magnification confocal microscopy and correlated with signal voids on MRI (Fig. 3). (a) Z-sectioning of the cell in the CPu (Figs. 3b and c) demonstrates the presence of Dil fluorescence throughout the cytoplasm and cell membrane. The presence of a solitary nucleus devoid of Dil (n) confirms the presence of a single cell. (b) Optical z-sectioning corresponding to the Dil fluorescence from one of the cells above the cc (Figs. 3e and f). Dil fluorescence occurs in two contiguous 25- $\mu\text{m}$  histologic sections. The z-sectioning data for each histologic section are shown as a separate row. Analysis of this cell indicates the presence of a solitary nucleus (n) that is continuous between the two contiguous histologic sections and is consistent with a single cell. 3D surface rendering of the z-section data for this cell (last column in b) shows the morphology of a single cell trapped at the bifurcation of a 6- $\mu\text{m}$  capillary. Scale bar (a,b) 10  $\mu\text{m}$ .

work, we show preliminary MR contrast measurements for cells labeled with  $60.9 \pm 1.6$  pg Fe/cell in mouse brain. With the *in vivo* scanning parameters used (SNR = 60, resolution =  $100 \times 100 \times 200 \mu\text{m}^3$ ), the average CNR for signal voids was  $\sim 14$ , which is above the minimum CNR of 5 required to detect signal voids against a uniform signal background (17). The  $\Delta S/S$  for signal voids in brain is shown to scale with resolution as predicted by previous studies of single cells in gelatin (18). Increasing spatial resolution should therefore provide improved cell detectability; however, prohibitively long scan times ( $\sim 6$  h) would be required to maintain an SNR of 60 at 1.5 T. Increasing field strength may provide additional SNR but overcoming off-resonance artifacts with FIESTA at higher field is not trivial. A number of groups, including our own, have now successfully implemented balanced SSFP at field strengths  $>4$  T (19,20). Further work will be required to determine whether improvements in single cell detection using balanced SSFP can be achieved at these higher field strengths.

We found a significant difference in the  $\Delta S/S$  for signal voids measured *in vivo* compared to formalin-fixed *ex vivo* brain. As well, there are significant differences between the magnitude of contrast generated by SPIO-labeled cells in brain and our previously published results for cells in gelatin (18). For example, controlling for imaging parameters, a cell loading of  $60.9 \pm 1.6$  pg Fe/cell is expected to generate  $\Delta S/S$  of  $\sim 0.7$  for cells in gelatin, which is significantly higher than the observed  $\Delta S/S$  of 0.227 and 0.280 for cells *in vivo* and *ex vivo*, respectively. It is not yet clear why such a discrepancy between these measurements exists but some possible explanations may be differences in SPIO loading or geometry of single cells entrapped in brain capillaries (e.g., due to loss of SPIO or stretching of cells) or differences in the FIESTA signal response for single cells in brain versus gelatin. The discordance in MR contrast measurements for single cells *in vitro* and *in vivo* may have significant implications for the detection limits of single SPIO-labeled cells in tissue compared to *in vitro* media such as gelatin or agarose. It also highlights the need for direct optical validation since a comparison of contrast measurements between single cells in gelatin and *in vivo* using the FIESTA pulse sequence cannot be used as proof of single cell detection. Further work will be required to ascertain the reasons for these differences and implications for the detection limit of single cells *in vivo* versus *in vitro*.

Our success in detecting single cells *in vivo* is the result of achieving simultaneously high resolution and high SNR images of the mouse brain in a scan time of approximately 90 min, making *in vivo* animal scanning practical. A significant advance that has allowed us to do this has been the implementation and optimization of the FIESTA pulse sequence in this microimaging application. This pulse sequence is extremely sensitive to the presence of cellularly compartmentalized SPIO (18,21), but possesses high SNR efficiency (19). In addition to pulse sequence optimization, improvements in MR hardware, specifically our implementation of high performance gradient coil technology and custom-fitted RF coils, is a significant factor in our successful demonstration of single cell sensitivity. The higher intrinsic SNR and resolution afforded by these op-

timized pulse sequence and hardware components are the chief contributing factors that have allowed us to achieve *in vivo* single cell detection despite the unconventionally low field strength used for microimaging in our experiments.

Currently, there is great interest in the longitudinal tracking of stem cell migration and homing. Similarly, there is much interest in monitoring the fate of solitary cancer cells as they invade tissue and begin to form metastases (22). The most common methods for analyzing these processes involve invasive, cross-sectional analyses on tissue by histopathology, or flow cytometric analysis. These techniques, however, provide only a static picture of the overall process and provide only a limited accounting of the fate of cells. For example, to determine the distribution of cells, the entire organ must be harvested and thin sectioned, followed by identification of individual cells by conventional microscopy. In contrast, the non-invasive nature of MRI combined with the single cell sensitivity demonstrated in this paper would allow for the localization and longitudinal tracking of single cells in entire organs without the need for tedious and time consuming histologic analyses. The ability to use MRI to follow cells noninvasively and longitudinally will therefore enable experiments that were previously impractical or impossible using any technique.

To date, we are unaware of any noninvasive *in vivo* imaging modality that possesses the whole body scope and single cell detection sensitivity of MRI. For example, the best cell tracking experiments that can be conducted with PET operate with a sensitivity of a few hundred cells (23). Similarly, *in vivo* whole body bioluminescence and fluorescence methods have a lower limit of cell detection in the range of hundreds to thousands of cells (24).

There are many questions that remain unanswered about single-cell MRI and its applications in biology. For example, the optimal choice of SPIO and loading method is not established. The loss of label and consequent reduction of single cell detectability as cells divide or die, and the time course over which the various SPIO particles are metabolized and broken down in different cell types, are not fully characterized and remain to be studied. Whether it will ever be possible to generate a stable superparamagnetic iron-based label within cells using reporter gene technology (25), at a labeling level sufficient for single cell detection, is an open question. The possibility of *in vivo* single cell detection in larger experimental animals and humans is an interesting and exciting possibility, made more conceivable through the proof-of-principle and use of clinical field strength embodied in this work. While we have met the requirements for single cell detection using an optimized high-powered gradient coil, which may not be completely translatable to the clinic, a number of groups have now demonstrated single cell detection *in vitro* on clinical MRI scanners without the need for specialized gradient hardware (26,27). The high SNR, high resolution, and time constraints required for single cell detection *in vivo*, however, mean that further development of methods and hardware are needed before single cell tracking can be performed in humans.

## ACKNOWLEDGMENTS

We thank Andrew Alejski and Yuteng Chen for technical support.

## REFERENCES

- Frangioni JV, Hajjar RJ. In vivo tracking of stem cells for clinical trials in cardiovascular disease. *Circulation* 2004;110:3378–3383.
- Bulte JW, Kraitchman DL. Iron oxide MR contrast agents for molecular and cellular imaging. *NMR Biomed* 2004;17:484–499.
- Massoud TF, Gambhir SS. Molecular imaging in living subjects: seeing fundamental biological processes in a new light. *Genes Dev* 2003;17:545–580.
- Hoehn M, Kustermann E, Blunk J, Wiedermann D, Trapp T, Wecker S, Focking M, Arnold H, Hescheler J, Fleischmann BK, Schwindt W, Buhrl C. Monitoring of implanted stem cell migration in vivo: a highly resolved in vivo magnetic resonance imaging investigation of experimental stroke in rat. *Proc Natl Acad Sci USA* 2002;99:16267–16272.
- Stroh A, Faber C, Neuberger T, Lorenz P, Sieland K, Jakob PM, Webb A, Pilgrimm H, Schober R, Pohl EE, Zimmer C. In vivo detection limits of magnetically labeled embryonic stem cells in the rat brain using high-field (17.6 T) magnetic resonance imaging. *Neuroimage* 2005;24:635–645.
- Dodd SJ, Williams M, Suhan JP, Williams DS, Koretsky AP, Ho C. Detection of single mammalian cells by high-resolution magnetic resonance imaging. *Biophys J* 1999;76:103–109.
- Lewin M, Carlesso N, Tung CH, Tang XW, Cory D, Scadden DT, Weissleder R. Tat peptide-derivatized magnetic nanoparticles allow in vivo tracking and recovery of progenitor cells. *Nat Biotechnol* 2000;18:410–414.
- Hinds KA, Hill JM, Shapiro EM, Laukkanen MO, Silva AC, Combs CA, Varney TR, Balaban RS, Koretsky AP, Dunbar CE. Highly efficient endosomal labeling of progenitor and stem cells with large magnetic particles allows magnetic resonance imaging of single cells. *Blood* 2003;102:867–872.
- Shapiro EM, Skrtic S, Koretsky AP. Sizing it up: cellular MRI using micron-sized iron oxide particles. *Magn Reson Med* 2005;53:329–338.
- Shapiro EM, Skrtic S, Sharer K, Hill JM, Dunbar CE, Koretsky AP. MRI detection of single particles for cellular imaging. *Proc Natl Acad Sci USA* 2004;101:10901–10906.
- Foster-Gareau P, Heyn C, Alejski A, Rutt BK. Imaging single mammalian cells with a 1.5 T clinical MRI scanner. *Magn Reson Med* 2003;49:968–971.
- Shapiro EM, Sharer K, Skrtic S, Koretsky AP. In vivo detection of single cells by MRI. In: *Proceedings of the 13th Annual Meeting of ISMRM*, Miami, 2005. p 13355.
- Wu YL, Foley LM, Williams JB, Ye Q, Horner JA, Hitchens TK, Ho C. Non-invasive direct in-vivo imaging of single immune cells in acute allograft rejection after heterotopic heart and lung transplantation in rats. In: *Proceedings of the 13th Annual Meeting of ISMRM*, Miami, 2005. p 132635.
- Bowen CV, Zhang X, Saab G, Gareau PJ, Rutt BK. Application of the static dephasing regime theory to superparamagnetic iron-oxide loaded cells. *Magn Reson Med* 2002;48:52–61.
- Frank JA, Miller BR, Arbab AS, Zywicke HA, Jordan EK, Lewis BK, Bryant LH, Jr., Bulte JW. Clinically applicable labeling of mammalian and stem cells by combining superparamagnetic iron oxides and transfection agents. *Radiology* 2003;228:480–487.
- Basse P, Hokland P, Heron I, Hokland M. Fate of tumor cells injected into left ventricle of heart in BALB/c mice: role of natural killer cells. *J Natl Cancer Inst* 1988;80:657–665.
- Rose A. The sensitivity performance of the human eye on an absolute scale. *J Opt Soc Am* 1948;38:196–208.
- Heyn C, Bowen CV, Rutt BK, Foster PJ. Detection threshold of single SPIO-labeled cells with FIESTA. *Magn Reson Med* 2005;53:312–320.
- Kohler S, Hiller KH, Griswold M, Bauer WR, Haase A, Jakob PM. NMR-microscopy with TrueFISP at 11.75T. *J Magn Reson* 2003;161:252–257.
- Lebel M, Menon RS, Bowen CV. Optimal balanced SSFP image recombination technique for suppression of banding artifacts surrounding surgical implants. In: *Proceedings of the 13th Annual Meeting of ISMRM*, Miami, 2005. p 132267.
- Scheffler K, Hennig J. Is TrueFISP a gradient-echo or a spin-echo sequence?. *Magn Reson Med* 2003;49:395–397.
- Chambers AF, Groom AC, MacDonald IC. Dissemination and growth of cancer cells in metastatic sites. *Nat Rev Cancer* 2002;2:563–572.
- Adonai N, Nguyen KN, Walsh J, Iyer M, Toyokuni T, Phelps ME, McCarthy T, McCarthy DW, Gambhir SS. Ex vivo cell labeling with <sup>64</sup>Cu-pyruvaldehyde-bis(N4-methylthiosemicarbazone) for imaging cell trafficking in mice with positron-emission tomography. *Proc Natl Acad Sci U S A* 2002;99:3030–3035.
- Troy T, Jekic-McMullen D, Sambucetti L, Rice B. Quantitative comparison of the sensitivity of detection of fluorescent and bioluminescent reporters in animal models. *Mol Imaging* 2004;3:9–23.
- Genove G, Demarco U, Xu H, Goins WF, Ahrens ET. A new transgene reporter for in vivo magnetic resonance imaging. *Nat Med* 2005;11:450–454.
- Zhang Z, van den Bos EJ, Wielopolski PA, de Jong-Popijus M, Duncker DJ, Krestin GP. High-resolution magnetic resonance imaging of iron-labeled myoblasts using a standard 1.5-T clinical scanner. *Magma* 2004;17:201–209.
- Pinkernelle J, Teichgraber U, Neumann F, Lehmkühl L, Ricke J, Scholz R, Jordan A, Bruhn H. Imaging of single human carcinoma cells in vitro using a clinical whole-body magnetic resonance scanner at 3.0 T. *Magn Reson Med* 2005;53:1187–1192.